Kinematics of the Most Efficient Cilium

Christophe Eloy[*] and Eric Lauga[†]

*Department of Mechanical and Aerospace Engineering, University of California San Diego,
9500 Gilman Drive, La Jolla, California 92093-0411, USA*
(Received 26 April 2012; published 17 July 2012)

In a variety of biological processes, eukaryotic cells use cilia to transport flow. Although cilia have a remarkably conserved internal molecular structure, experimental observations report very diverse kinematics. To address this diversity, we determine numerically the kinematics and energetics of the most efficient cilium. Specifically, we compute the time-periodic deformation of a wall-bound elastic filament leading to transport of a surrounding fluid at minimum energetic cost, where the cost is taken to be the positive work done by all internal molecular motors. The optimal kinematics are found to strongly depend on the cilium bending rigidity through a single dimensionless number, the Sperm number, and closely resemble the two-stroke ciliary beating pattern observed experimentally.

Cilia are slender filaments, typically a few microns in length, used by eukaryotic cells to transport or sense flows [1,2]. Familiar examples include those densely packed on the surface of *Paramecia* enabling locomotion [1], the cilia covering our airways and helping expel mucus toward the pharynx [3], or those responsible of the left-right symmetry breaking during embryonic development [4].

The cilium internal structure has been highly conserved throughout evolution. It generally consists of a central pair of microtubules surrounded by nine microtubule doublets, to form the so-called "9 + 2" structure [5]. Deformation of the cilium is achieved by the action of ATP-fueled protein motors (dynein) that generate internal torques from the relative sliding of adjacent microtubule doublets. Yet, the mechanisms that regulate dynein activity and thus ciliary deformation are not well understood [6].

The beating cycle of a cilium typically consists of two phases (Fig. 1, left): an effective stroke aimed at generating flow, during which the cilium is almost straight while moving in a plane normal to the cell surface, and a recovery stroke, during which the cilium returns to its initial position by exhibiting large curvatures and possibly moving out of the normal plane. Past experimental studies have shown that cilia from different cells can exhibit qualitatively different kinematics [1]. However, the parameters, physical or biological, that select or constrain these kinematics are still unknown.

In this Letter, we address this open question by computing the optimal kinematics of an elastic cilium attached to a wall, i.e., the time-varying deformation that minimizes the energetic cost for a given transport of the surrounding fluid. Recent work focused on the optimal deformation of flagellated cells [7] and cilia [8] by minimizing the energy lost to viscous dissipation in the fluid. Here, we argue that one needs to rigorously consider the internal structure of the cilia and measure the energetic costs as the sum of the positive work done by internal molecular torques, similar

to the current models of muscle energetics [9]. This modeling approach leads to optimal ciliary kinematics displaying the experimentally observed two-stroke cycle and strongly dependent on the cilium bending rigidity.

The cilium is modeled as an inextensible elastic filament of length L and radius a, clamped normally into the plane Oxy (Fig. 1). The filament centerline is described by the vector $\mathbf{r}(s, t)$, where s is the curvilinear coordinate, and the material frame $(\mathbf{d}_1, \mathbf{d}_2, \mathbf{d}_3)$ describes the local orientation of the filament, with $\mathbf{d}_3 = \mathbf{r}'$ the tangential unit vector, such that

$$\mathbf{d}_i' = \mathbf{D} \times \mathbf{d}_i, \qquad \dot{\mathbf{d}}_i = \boldsymbol{\Omega} \times \mathbf{d}_i, \quad \text{for } i = 1 \cdots 3, \qquad (1)$$

where the primes and dots note the differentiation with respect to s and t, respectively, $\mathbf{D}$ is the Darboux vector [10,11], and $\boldsymbol{\Omega}$ the angular velocity.

The balance of forces and moments on a cross section are expressed by the Kirchhoff equations for a rod [11]

$$\mathbf{T}' - \mathbf{F} = 0, \qquad \mathbf{M}' + \mathbf{d}_3 \times \mathbf{T} + \mathbf{q} = 0, \qquad (2)$$
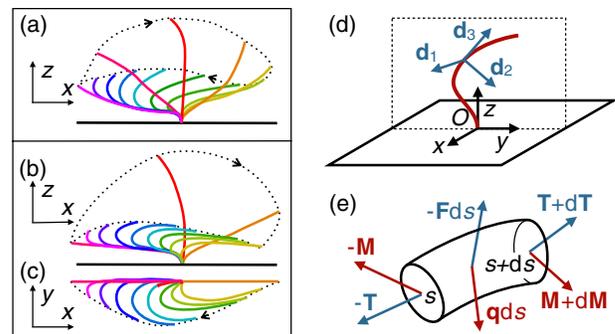

FIG. 1 (color online). Typical two-dimensional (a) and three-dimensional (b),(c) cilium kinematics as observed for *Pleurobrachia* [24] and *Mytilus edulis* [25], respectively. Sketch of the coordinates (d) and of the forces and moments that apply on a filament element ds (e).

supplemented by clamped-free boundary conditions, where **T** and **M** are the internal tension and bending moment, respectively, and $-\mathbf{F}$ is the fluid drag per unit length (opposite to the force density **F** exerted by the filament on the surrounding fluid). In the relevant slender limit $a/L \ll 1$, the internal forces generated by the dynein arms contribute, at first order, to an active torque per unit length, **q**, as in Eq. (2) [12]. Since the energy needed to produce torsion is of order L/a larger than that to produce bending [13], the tangential component of this internal torque can be neglected, $\mathbf{q} \cdot \mathbf{d}_3 = 0$, which yields no twist of the filament, $\mathbf{D} \cdot \mathbf{d}_3 = 0$.

The Hookean constitutive relation relates the bending moment **M** to the Darboux vector **D** through a linear relation. In the absence of torsion and for an axisymmetric filament, it simplifies to $\mathbf{M} = B\mathbf{D} = B\mathbf{d}_3 \times \mathbf{d}_3'$, with B the bending rigidity. Combining this constitutive relation, the free boundary condition at $s = L$, and Eq. (2), the internal torque **q** can be expressed as a function of $\mathbf{d}_3$ and **F** alone:

$$\mathbf{q} = B\mathbf{d}_3'' \times \mathbf{d}_3 + \mathbf{d}_3 \times \int_s^L \mathbf{F}(u)du. \qquad (3)$$

Assuming the cilium kinematics is known, we need to evaluate the hydrodynamic forces **F** in order to fully determine the internal torque **q**. Since the cilia are few microns long, their Reynolds number is small and the surrounding flow follows the Stokes equations. In this limit, $\mathbf{F}(s)$ represents a distribution of stokeslets, which are the Green functions (point forces) of the Stokes equations.

Taking advantage of the small aspect ratio of the filament, we use the slender-body theory [14,15], which allows us to linearly relate $\mathbf{F}(s)$ to the instantaneous distribution of velocities $\dot{\mathbf{r}}(s)$ along the cilium centerline. To take into account the presence of the no-slip wall to which the cilium is anchored, slender-body theory is supplemented with Blake's system of hydrodynamic images [16], allowing us to formally write

$$\dot{\mathbf{r}}(s) = L_{\text{RFT}} \cdot \mathbf{F} + L_{\text{SBT}}(\mathbf{F}) + L_{\text{image}}(\mathbf{F}), \qquad (4)$$

where L_{RFT} is the local linear operator of the so-called resistive-force theory [2], given by $L_{\text{RFT}} = (\mathbf{1} + \mathbf{d}_3\mathbf{d}_3)/\xi_\perp$, with **1** the 3×3 identity matrix, $\xi_\perp = 4\pi\mu/\ln(L/a)$, and μ the dynamic viscosity of the fluid. The linear integral operators L_{SBT} and L_{image}, which are of order $\ln(L/a)$ smaller, account for the cilium-cilium and cilium-wall hydrodynamic interactions, respectively. Their full expressions can be found in Refs. [14,16]. Numerically, Eq. (4) is regularized by using Legendre polynomials to diagonalize the singular part of L_{SBT} [15]. Once this regularization is performed, the discretization and inversion of Eq. (4) is straightforward. The resulting computational implementation of Eq. (4) is correct to the order $O[(a/L)^2 \ln(L/a)]$ [14].

Without loss of generality, the net flow transported by the cilium is assumed to occur in the x direction. This transport is quantified by the flow rate, Q, across the Oyz half-plane (Fig. 1), which, by virtue of incompressibility, is equal to the flow rate through any parallel half-plane, and can thus be evaluated in the far field for convenience [8]. Far from the filament, the flow is dominated by the contribution of stokeslets along the cilium, $\mathbf{F}(s)$, and their images, which consist of stokeslets, force dipoles, and source dipoles [16]. Combined together, these singularities are equivalent at leading order to a symmetric combination of two force dipoles located in O, known as a stresslet [17], leading to a flow rate given by

$$Q = \frac{1}{\pi\mu}\left\langle \int_0^L F_x r_z ds \right\rangle, \qquad (5)$$

where the brackets denote time averaging.

The power expended to convert ATP into work with the molecular motors is then assumed to be proportional to the mechanical power, P, consumed by the internal torques, **q**, where only positive work is accounted for [9]:

$$P = \left\langle \int_0^L \max(0, \mathbf{q} \cdot \mathbf{\Omega})ds \right\rangle. \qquad (6)$$

Distinguishing between the positive and negative work means that the dynein arms cannot harvest energy, which breaks the conservative nature of elastic energy. The mean power spent by the internal torque is thus larger than the power given to the fluid; i.e., $P \gtrsim \langle \int_0^L \mathbf{F} \cdot \dot{\mathbf{r}}ds \rangle$.

From the definition of the flow rate, Q, and the mean mechanical power, P, a dimensionless efficiency can be constructed similarly to the one proposed in Ref. [8] as

$$\eta = Q^2\mu^2/(P\xi_\perp L^3). \qquad (7)$$

With this definition, the transport efficiency, η, does not depend on the beat angular frequency, ω, or on the aspect ratio at first order, since the flow rate scales as $Q \sim \omega L^3 \xi_\perp/\mu$ and the power as $P \sim \xi_\perp \omega^2 L^3$.

Dimensional analysis shows that the problem is entirely governed by two dimensionless numbers. The first is the aspect ratio of the cilium, L/a. The cilia covering the body of *Paramecium* have $L \approx 12 \, \mu$m and $a \approx 0.12 \, \mu$m, so we assume that $L/a = 100$. Note that since the aspect ratio appears only logarithmically in the problem through Eq. (4), its influence is essentially negligible. The second dimensionless number is the Sperm number, introduced by Lagomarsino *et al.* [18] as

$$\text{Sp} = L(\omega\xi_\perp/B)^{1/4}, \qquad (8)$$

which measures the ratio between the cilium length and the elasto-viscous penetration length. The kinematics of optimal ciliary motion depend strongly on the value of Sp. For *Paramecium*, the angular frequency is $\omega \approx 200 \, \text{rad s}^{-1}$ [1], and with the bending rigidity estimated to be $B = 25 \, \text{pN} \, \mu\text{m}^2$ [19], one obtains $\text{Sp} \approx 4.6$ in water. Some cilia are shorter, such as the nodal cilia involved in embryonic development with $L \approx 2.5 \, \mu$m for mice [20] and $L \approx 5 \, \mu$m for humans [4], corresponding to $\text{Sp} \approx 1$ and $\text{Sp} \approx 2$, respectively. Other cilia can be much longer, reaching hundreds of microns (thus $\text{Sp} > 100$), such as the
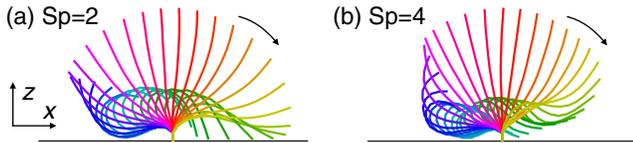
FIG. 2 (color online).   Two-dimensional optimal ciliary motions for Sp = 2 (a) and Sp = 4 (b). The stroboscopic views show the cilium every 1/32 of the period. The energy dissipated in the fluid represents, respectively, 38% and 90% of the total energetic costs for Sp = 2 and Sp = 4.

cilium of *Pleurobrachia* reproduced in Fig. 1(a). In this Letter, we focus on the range $1 \le \mathrm{Sp} \le 7$, corresponding approximately to cilia of lengths $2.5 \lesssim L \lesssim 18$ μm, for which the most drastic changes appear in optimal kinematics.

For given values of both L/a and Sp, the cilium kinematics that maximizes the pumping efficiency, η, is computed numerically. The elastic filament is first discretized as an assembly of n_s discrete rods connected by springs [21], and the stokeslet distribution is evaluated n_t times per cycle. The values $n_s = 16$ and $n_t = 32$ have been used in this study and allow us to evaluate the efficiency of a given kinematics rapidly without compromising precision. The filament kinematics is parametrized by imposing the curvatures at N_s points along the filament centerline N_t times per period. The curvatures on the $n_s \times n_t$ points are then interpolated with a cubic spline from those $N_s \times N_t$ points. Our results are obtained with $N_s = N_t = 6$, giving 36 and 72 degrees of freedom in two and three dimensions, respectively, and the optimal kinematics are computed using a sequential programming (SQP) algorithm. A preliminary optimum can be found using the resistive-force theory only (i.e., neglecting the last two terms in Eq. (4)), which is qualitatively similar to the optimum found with the full hydrodynamics, but at a much lower cost. This preliminary optimum can then be used as an initial guess in full hydrodynamics optimization. Our numerical approach is validated by a comparison with the results of Ref. [8] obtained with a bead model and an energetic measure of the dissipation in the fluid only. The transport efficiency in Ref. [8] is $\eta = 0.0035$, corresponding to the large values of Sp here and comparing well with our optimum for Sp = 7, $\eta = 0.0033$.

Optimal two-dimensional kinematics are displayed in Fig. 2 for Sp = 2 and 4. We see that our optimization approach, which rigorously quantifies the internal work expended by molecular motors, leads to kinematics with the experimentally observed two-stroke cycle: an effective stroke during which the filament is rotating almost rigidly around its anchor point, and a recovery stroke exhibiting large curvatures. The energy dissipated in the fluid represents only a fraction of the total energetic costs (this fraction increases with Sp: from 5% for Sp = 1, to 38% for Sp = 2, to 90% for Sp = 4). For small values of Sp (short or stiff cilia), the curvature is essentially always of the same sign [Fig. 2(a)], whereas for larger values of Sp (long or flexible cilia), the curvatures are larger and occasionally change their sign [Fig. (2(b))]. In order to minimize backflow during the recovery stroke, the trajectory has to be as close to the wall as possible, and in order to achieve such a trajectory, large curvatures with high energetic costs are necessary; the resulting optimum is thus a balance, tuned by the value of Sp, between the distance to the wall and curvature.

The optimal three-dimensional ciliary kinematics have also been determined. The results are illustrated in Fig. 3 for Sp = 1, 2, and 4. For small values of Sp, the cilium is rotating around an axis inclined at an angle of approximately 45 degrees with respect to the surface normal [Fig. 3(a)]. This optimal motion is similar to the observed trajectories of nodal cilia [4]. For larger values of Sp, the optimal cilium kinematics break the $x \rightarrow -x$ symmetry, and, as in two-dimensional case, the motion can be decomposed into an effective stroke in the vertical plane and a recovery stroke with large curvatures. During the recovery stroke, the filament takes advantage of the third dimension to achieve a trajectory closer to the wall, and therefore is more efficient than in the two-dimensional case. These three-dimensional optimal kinematics reproduce the experimental observations of real cilia motions, as can be seen by comparing the kinematics of *Mytilus edulis* [Figs. 1(b) and 1(c)] with Fig. 3(c), for instance. For Sp = 4, the mechanical power expanded to produce the optimal kinematics is $P = 0.13 \xi_\perp \omega^2 L^3$, which gives for a typical cilium of *Paramecium*, $P \approx 2.5 \times 10^{-14}$ W, in agreement with experimental observations [22].
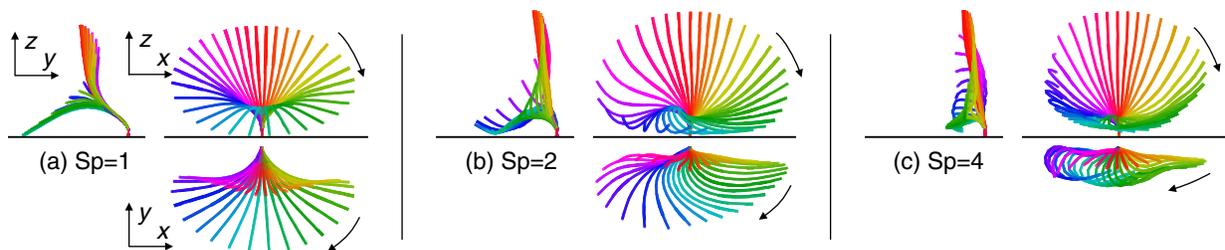

FIG. 3 (color online).   Three-dimensional optimal ciliary motions for Sp = 1 (a), Sp = 2 (b), and Sp = 4 (c). The fractions of energy dissipated in the fluid are, respectively, 79%, 92%, and 99% of the total energetic costs for Sp = 1, Sp = 2, and Sp = 4.

It is to be noted that the value of the efficiency remains unchanged for a given filament kinematics by the transformations $x \rightarrow -x$, $y \rightarrow -y$, or $t \rightarrow -t$. The same flow direction and efficiency could thus be obtained with clockwise or counterclockwise rotations (by a y reflection), and with the bend forward or tip forward during the recovery stroke (by combining x and t reflections). For the real cilia, however, chirality generally constrains the motion to be clockwise.

The influence of the value of Sp on the optimal pumping efficiency is illustrated in Fig. 4, both for two- and three-dimensional motions. As expected, three-dimensional deformation is more efficient for all Sp since the number of degrees of freedom is larger, although the two cases converge to similar efficiencies for large Sp. In both cases, efficiency is a monotonically increasing function of the Sperm number: increasing Sp is equivalent to reducing the bending rigidity and thus allowing larger curvatures for a lower energetic cost. In fact, the mean square curvature of the motion appears to be almost an exponential function of Sp in the range studied (inset of Fig. 4). Unless an artificial dissipative term is introduced, one can thus expect the problem to become mathematically ill posed in the limit of a large Sp, which is equivalent to considering only the energy dissipated in the fluid [8].

Interestingly, although an increase in bending rigidity generally increases the energetic cost, it is not always strictly true. Using the kinematics shown in Fig. 3(b) corresponding to the optimum for Sp = 2, "freezing" it, and varying Sp, one finds the maximum efficiency when Sp = 3.2. However, this efficiency is only 0.05% larger than the efficiency for Sp = ∞, and obviously a larger efficiency can be achieved at Sp = 3.2 if the kinematics is allowed to vary. This result shows that bending of the cilium allows the storage of elastic energy that can be restored later in the motion.

As discussed above, we assumed that active internal torques have no tangential components due to their prohibitive cost in the slender limit, $a/L \ll 1$. As a result, and
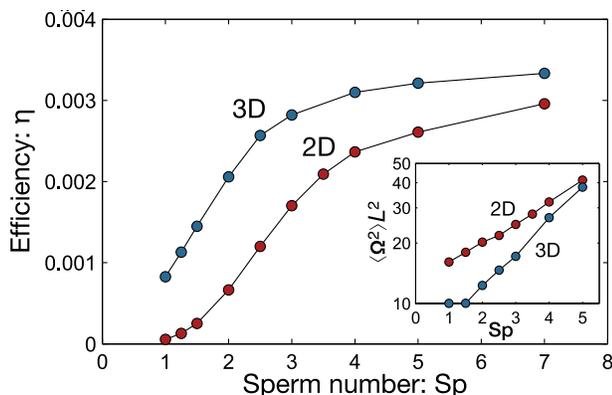
because the cilium is assumed to be axisymmetric, optimization always yields kinematics with zero twist. Even if a more realistic model were adopted with slightly different bending rigidities along the $\mathbf{d}_1$ and $\mathbf{d}_2$ directions owing to the central microtubule pair, the twist would not be larger than few degrees due to the large twist rigidity [13]. In addition, even when torsion is not present, the filament kinematics can give the illusion of twist, since its extremity rotates, as shown in Fig. 5. This classical result of differential geometry [10,11] can explain why some studies reported the presence of twist on the cilia of *Paramecium* [23].

In summary, we have proposed in this Letter that, in order to derive the appropriate efficiency of cilia-driven fluid transport, the detailed internal structure of cilia has to be considered, and energetic costs have to be calculated as the sum of the positive work done by the internal torques. Using this approach, we have developed a numerical model that allows us to compute the kinematics of a wall-bound elastic cilium transporting the surrounding fluid at minimum energetic cost. The optimal motions of the cilium have been found to strongly depend on its bending rigidity through a single-dimensionless parameter, Sp. These optimal kinematics were found to display the experimentally observed two-stroke cycle in both the two- and three-dimensional motions. A large part of the total energy consumed by a cell can be devoted to flow transport, in particular for large eukaryotes. For instance, 70% of the energy in *Paramecium* is estimated to be used for swimming [22]. In the human body, the average power expended by a single cell is approximately 10^{-11} W and is equal to that required to actuate between a hundred and a thousand cilia. Given these requirements, it is therefore quite possible that cilia kinematics have evolved to minimize the internal energy expenditure.

Although we have focused our study on the case of a single filament, cilia in biology are generally densely packed on surfaces, and as such are strongly influenced by hydrodynamical interactions with their neighbors. These interactions are an intriguing avenue for future work: they could affect flow transport and be responsible for the different cilium velocities observed during effective and recovery strokes [8].
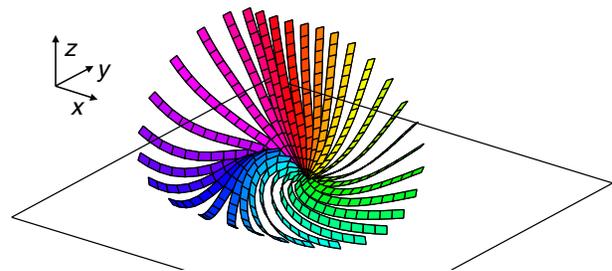

FIG. 4 (color online). Optimal pumping efficiency, η, as a function of Sp, for two- (2D) and three-dimensional (3D) cilium kinematics. The inset shows the variation of the mean square curvature for the optimal kinematics (semilog scale).

FIG. 5 (color online). Illusion of twist for Sp = 2. The three-dimensional kinematics is plotted as if the filament was a ribbon to emphasize the orientation of $\mathbf{d}_1$.

————————

*eloy@irphe.univ-mrs.fr
Permanent address: Aix–Marseille University, IRPHE, CNRS, Marseille, France.
†elauga@ucsd.edu

[1] *Cilia and Flagella*, edited by M. A. Sleigh (Academic Press, London, New York, 1974).
[2] E. Lauga and T. R. Powers, Rep. Prog. Phys. **72,** 096601 (2009).
[3] M. A. Sleigh, J. R. Blake, and N. Liron, Am. Rev. Respir. Dis. **137,** 726 (1988).
[4] N. Hirokawa, Y. Okada, and Y. Tanaka, Annu. Rev. Fluid Mech. **41,** 53 (2009).
[5] P. Satir and S. T. Christensen, Annu. Rev. Physiol. **69,** 377 (2007).
[6] C. B. Lindemann and K. A. Lesich, J. Cell Sci. **123,** 519 (2010).
[7] D. Tam and A. E. Hosoi, Proc. Natl. Acad. Sci. U.S.A. **108,** 1001 (2011).
[8] N. Osterman and A. Vilfan, Proc. Natl. Acad. Sci. U.S.A. **108,** 15727 (2011).
[9] R. M. Alexander, Phil. Trans. R. Soc. B **338,** 189 (1992).
[10] T. R. Powers, Rev. Mod. Phys. **82,** 1607 (2010).
[11] B. Audoly and Y. Pomeau, *Elasticity and Geometry* (Oxford University Press, Oxford, 2010).
[12] A. Hilfinger and F. Jülicher, Phys. Biol. **5,** 016003 (2008).
[13] M. Hines and J. J. Blum, Biophys. J. **47,** 705 (1985).
[14] R. E. Johnson, J. Fluid Mech. **99,** 411 (1980).
[15] T. Götz, Ph.D. thesis, Universität Kaiserslautern, 2000.
[16] J. R. Blake, Proc. Cambridge Philos. Soc. **70,** 303 (1971).
[17] G. Batchelor, J. Fluid Mech. **41,** 545 (1970).
[18] M. C. Lagomarsino, F. Capuani, and C. P. Lowe, J. Theor. Biol. **224,** 215 (2003).
[19] M. Hines and J. J. Blum, Biophys. J. **41,** 67 (1983).
[20] J. H. E. Cartwright, O. Piro, and I. Tuval, Proc. Natl. Acad. Sci. U.S.A. **101,** 7234 (2004).
[21] M. Bergou, M. Wardetzky, S. Robinson, B. Audoly, and E. Grinspun, ACM Trans. Graph. **27,** 63 (2008).
[22] Y. Katsu-Kimura, F. Nakaya, S. A. Baba, and Y. Mogami, J. Exp. Biol. **212,** 1819 (2009).
[23] C. K. Omoto and C. Kung, J. Cell Biol. **87,** 33 (1980).
[24] M. A. Sleigh, Symp. Soc. Exp. Biol. **22,** 131 (1968).
[25] E. Aiello and M. A. Sleigh, J. Cell Biol. **54,** 493 (1972).